Design and Analysis of a New 7-DOF Parallel Type Haptic Device : PATHOS-II

Keehoon Kim Wan Kyun Chung Youngil Youm

Robotics & Bio-Mechatronics Lab., Pohang University of Science and Technology(POSTECH) , Pohang, Korea
Tel : +82-54-279-2844, Fax : +82-54-279-5899, E-mail : {khk,wkchung,youm}@postech.ac.kr

***Abstract*— Most tele-operation to manipulate an object consists of grasping and manipulation, and two or more 6-DOF haptic devices are usually used in master side. In this article, a new simply designed 7-DOF haptic device, PATHOS II is proposed for 1-DOF grasping and 6-DOF manipulation. The merits of a parallel type haptic device such as high stiffness and accuracy are natural characteristics of PATHOS-II with optimized workspace. Due to its unique symmetric structure, the isotropic manipulability is enhanced within the reachable workspace. This parallel type haptic device can be used in applications which need high precision, stiffness and isotropic manipulability.**

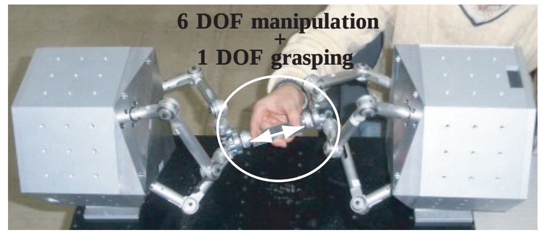

Fig. 1. 7-DOF motion of PATHOS-II

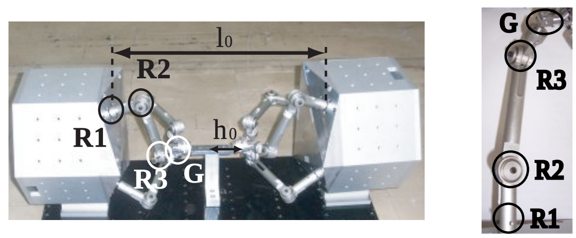

Fig. 2. PATHOS-II and its leg

I. Introduction

A haptic device is an instrument which conveys operator's command to slave manipulator and produces kinesthetic sensation to make an operator feel the situation of slave side. Recently, the number of applications of tele-operation is growing in various fields of micro manipulation, tele-surgery, virtual training, and outdoor robotics. Haptic devices can be classified into glove type[1], exoskeleton type[2], and pen type[3] by the way of transmitting sensation, or serial type[3], parallel type[4], and magnetic levitation type[5] by the way of generating sensation. The type of haptic device is determined by the purpose of their required function.

In tele-operation, most procedures are : the operator moves the slave manipulator near the target, grasps the object, and manipulates it. For the purpose of the task, two 6 DOF haptic devices are usually used. However, it is redundant to use two haptic devices for the task. In this article, a new parallel type haptic device for 6-DOF motion and 1-DOF grasping with force reflection, PATHOS-II(Postech pArallel Type Haptics Operating System), is proposed. Figure 1 shows that it is possible to do the task with a PATHOS-II.

The most important reason to use parallel structure for a haptic device is its high stiffness compared to any other types. With the characteristics, the haptic device can not only display high force feedback but also generate elaborate motion. In spite of the merits, there are tradeoffs like complex kinematics, small workspace, isotropy, and singularity problems.

PATHOS-II is designed simply with only revolute joints to minimize above mentioned complex kinematics. Since it has simple structure, it is easy to solve kinematics and computational load becomes lower. Especially, with only 9 sensors among 25 joints, forward kinematics of 7-DOF is obtained easily as will be stated in section 2. In order to maximize the workspace of PATHOS-II, link ratio and initial orientation are optimized. The workspace covers the human haptic manipulation[7] in section 3.

Isotropy is another important factor to determine whether the designed device can be used as a haptic device. In order to guarantee similar isotropic stiffness, PATHOS-II was designed to have symmetric structure. Active joint direction vector is also considered. As a result, uniform isotropic property of PATHOS-II is mentioned in section 4.

Since PATHOS-II has parallel type structure, high stiffness is the natural characteristics. With its high stiffness, accurate kinesthetic haptic display can be achieved and high precision operation is possible. The stiffness of PATHOS-II is verified by the experiments in section 5 and conclusion follows.

II. Kinematics

PATHOS-II was designed symmetrically with 6 legs which consist of only revolute joints and as a result, the kinematics is simple to solve. In this section, structure of PATHOS-II is explained and inverse and forward kinematics with 9 sensors will be shown.

A. System Description

A leg of PATHOS-II has 3 revolute joints and 1 globular joint as shown in Figure 2. A globular joint consists of 3 revolute joints as shown in Figure 3. The revolute joint at the end of a leg, $R1$, is fixed on base plate and the globular joint is fixed on top plate. The number in circles on base plates denotes the position of leg. globular joints are also located on top plate in the same order. Then, PATHOS-II has 21 links(3 links in each leg, 1 base plate, and 2 top plates) and 25 joints(1 globular and 3 revolute joints in each leg and a joint between top plates). From

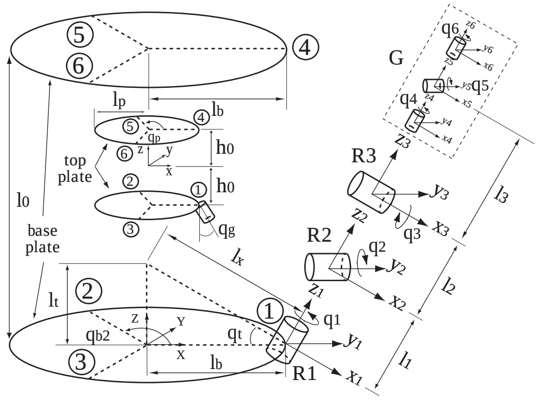

Fig. 3. Structure of PATHOS-II

Freudenstein and Maki's method[6] for spatial mechanism[1],

$$\begin{aligned} F &= 6(L-J-1)+\sum_{i=1} f_i \\ &= 6(21-25-1)+1\times 3\times 6+3\times 6+1\times 1 \\ &= 7(\text{DOF}). \end{aligned}$$

The first joints of each leg, $R1$ in Figure 2, are active joints. h_0 is half of distance between top plates in Figure 3. h_0 is changed by an operator grasping motion. Therefore, PATHOS-II needs 6 actuators at the first joints of each leg and one between top plates for force feedback. If h_0 becomes constant when an operator grasps an object,

$$\begin{aligned} F &= 6(20-24-1)+1\times 3\times 6+3\times 6 \\ &= 6(\text{DOF}), \end{aligned}$$

and 6DOF manipulation of an object is possible.

B. Inverse Kinematics

In Figure 3, $X-Y-Z$ coordinate at the center of base plate is the reference and $x-y-z$ coordinate fixed at the center of top plates is used to describe the pose of end effector. Those coordinates are common to every leg.

One leg has the following transformation from reference coordinate to the pose of end effector.

$$\begin{aligned} \boldsymbol{T} = \quad & \{T_z(L)R_x(\theta_{b1})R_z(\theta_{b2})T_z(l_t)R_y(\theta_t)T_x(l_x)\} \\ & R_z(\theta_1)T_z(l_1)R_y(\theta_2)T_z(l_2)R_x(\theta_3)T_z(l_3)R_z(\theta_4) \\ & R_y(\theta_5)R_x(\theta_6)\{R_x(\theta_{b1})T_z(-h_0)R_z(\theta_p)T_x(l_p) \\ & R_y(\theta_g)\}^{-1}. \end{aligned} \tag{1}$$

T and R in Eq.(1) are homogeneous transforms which indicate translation and rotation. T_x means translation in x direction and R_x means rotation about x axis. L is 0 for 1st to 3rd leg and l_0 for 4th to 6th leg. l_0 is the distance between base plates. θ_{b1} is 0° for 1st to 3rd leg and 180° for 4th to 6th leg. Other variables in Eq.(1) are shown in Figure 3. If the system is determined, all terms of Eq.(1) are known except $\theta_i (i=1,2,3,4,5,6)$.

From Eq.(1), we can find the position closure and position vector, $\boldsymbol{a}$ in Eq.(2) is known.

$$R_z(\theta_1)T_z(l_1)R_y(\theta_2)T_z(l_2)R_x(\theta_3)T_z(l_3) = \begin{bmatrix} \times & \boldsymbol{a} \\ \boldsymbol{0} & 1 \end{bmatrix}. \tag{2}$$

[1] F is degree of freedom, L is number of links, J is number of joints, and f_i is degree of freedom of ith joint

Hereafter, R and T denote orientation and translation part of homogeneous transform respectively. R is a 3×3 matrix and T is a 3×1 vector. Then, Eq.(2) becomes

$$R_z(\theta_1)[T_z(l_1)+R_y(\theta_2)\{T_z(l_2)+R_x(\theta_3)T_z(l_3)\}] = \boldsymbol{a}. \tag{3}$$

Eq.(3) can be represented by the following 3 equations.

$$\begin{aligned} R_z(\theta_1)\boldsymbol{C}_1 &= \boldsymbol{a}, \\ R_y(\theta_2)\boldsymbol{C}_2 &= \boldsymbol{C}_1 - T_z(l_1), \\ R_x(\theta_3)T_z(l_3) &= \boldsymbol{C}_2 - T_z(l_2). \end{aligned} \tag{4}$$

In matrix form, it is

$$\begin{bmatrix} C\theta_1 & -S\theta_1 & 0 \\ S\theta_1 & C\theta_1 & 0 \\ 0 & 0 & 1 \end{bmatrix} \begin{bmatrix} c_{1x} \\ c_{1y} \\ c_{1z} \end{bmatrix} = \begin{bmatrix} a_x \\ a_y \\ a_z \end{bmatrix}, \tag{5}$$

$$\begin{bmatrix} C\theta_2 & 0 & S\theta_2 \\ 0 & 1 & 0 \\ -S\theta_2 & 0 & C\theta_2 \end{bmatrix} \begin{bmatrix} c_{2x} \\ c_{2y} \\ c_{2z} \end{bmatrix} = \begin{bmatrix} c_{1x} \\ c_{1y} \\ c_{1z}-l_1 \end{bmatrix}, \tag{6}$$

$$\begin{bmatrix} 1 & 0 & 0 \\ 0 & C\theta_3 & -S\theta_3 \\ 0 & S\theta_3 & C\theta_3 \end{bmatrix} \begin{bmatrix} 0 \\ 0 \\ l_3 \end{bmatrix} = \begin{bmatrix} c_{2x} \\ c_{2y} \\ c_{2z}-l_2 \end{bmatrix}. \tag{7}$$

$C\theta_i$ and $S\theta_i$ denote $\cos\theta_i$ and $\sin\theta_i$. From Eq.(5-7), the equivalent 6 equations are

$$c_{1z} = a_z, \tag{8}$$

$$\begin{bmatrix} C\theta_1 \\ S\theta_1 \end{bmatrix} = \frac{1}{c_{1x}^2+c_{1y}^2} \begin{bmatrix} c_{1x} & c_{1y} \\ -c_{1y} & c_{1x} \end{bmatrix} \begin{bmatrix} a_x \\ a_y \end{bmatrix}, \tag{9}$$

$$c_{2y} = c_{1y}, \tag{10}$$

$$\begin{bmatrix} C\theta_2 \\ S\theta_2 \end{bmatrix} = \frac{1}{c_{2x}^2+c_{2z}^2} \begin{bmatrix} c_{2x} & c_{2z} \\ c_{2z} & -c_{2x} \end{bmatrix} \begin{bmatrix} c_{1x} \\ c_{1z}-l_1 \end{bmatrix}, \tag{11}$$

$$c_{2x} = 0, \tag{12}$$

$$\begin{bmatrix} C\theta_3 \\ S\theta_3 \end{bmatrix} = \frac{1}{l_3} \begin{bmatrix} c_{2z}-l_2 \\ -c_{2y} \end{bmatrix}. \tag{13}$$

After some calculation with Eq.(8) to (13), coefficients are determined as following.

$$\begin{aligned} c_{1x} &= \pm\sqrt{a_x^2+a_y^2-c_{1y}^2}, \\ c_{1y} &= c_{2y} = \pm\sqrt{l_3^2-(c_{2z}-l_2)^2}, \\ c_{1z} &= a_z, \\ c_{2x} &= 0, \\ c_{2y} &= \pm\sqrt{l_3^2-(c_{2z}-l_2)^2}, \\ c_{2z} &= \{l_2^2-l_3^2+a_x^2+a_y^2+(a_z-l_1)^2\}/2l_2. \end{aligned} \tag{14}$$

Then, θ_1, θ_2, and θ_3 are solved from Eq.(9), (11), and (13) with coefficients in Eq.(14). Then, in Eq.(1), 3 terms, θ_4, θ_5, and θ_6, are unknown. To find them, the following equations are derived from Eq.(1).

$$R_z(\theta_4)R_y(\theta_5)R_x(\theta_6) = B = \begin{bmatrix} b_{11} & b_{12} & b_{13} & 0 \\ b_{21} & b_{22} & b_{23} & 0 \\ b_{31} & b_{32} & b_{33} & 0 \\ 0 & 0 & 0 & 1 \end{bmatrix}. \tag{15}$$

The matrix B is known from Eq.(1). After multiplying

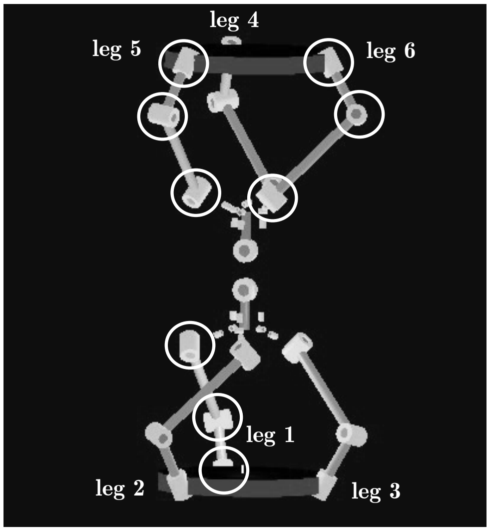

Fig. 4. The location of sensors

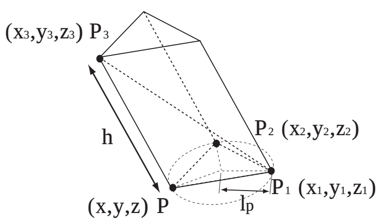

Fig. 5. Top plate and positions of globular joints of 1st(P_3), 5th(P_2), 6th(P_1), and 4th leg(P)

$R_z(\theta_4)^{-1}$,

$$\theta_4 = \tan^{-1}\left(\frac{b_{23}}{b_{13}}\right), \tag{16}$$

$$\begin{bmatrix} C\theta_5 \\ S\theta_5 \end{bmatrix} = \begin{bmatrix} b_{33} \\ b_{13}C\theta_4 + b_{23}S\theta_4 \end{bmatrix}, \tag{17}$$

$$\begin{bmatrix} C\theta_6 \\ S\theta_6 \end{bmatrix} = \begin{bmatrix} -b_{12}S\theta_4 + b_{22}C\theta_4 \\ -b_{11}S\theta_4 + b_{21}C\theta_4 \end{bmatrix}. \tag{18}$$

These give θ_4, θ_5, and θ_6, and this procedure is applied to every leg.

C. Forward Kinematics

Forward kinematics is to find the pose of top plate, $\boldsymbol{T}$, and h_0 in Eq.(1) from the sensor information. PATHOS-II uses 9 sensors to solve 7-DOF forward kinematics.

The locations of sensors are shown in Figure 4. In Eq.(1), $\boldsymbol{T}$ and h_0 for 1st, 5th, and 6th leg are unknown. The positions of globular joints, $\boldsymbol{a}$ in Eq.(2), of 1st, 5th, and 6th leg can be calculated from 9 sensors in Figure 4. Then, Figure 5 shows the top plate. Vertices mean the positions of globular joints of each leg. In other words, $P1(x1, x2, x3)$, $P2(x2, y2, z2)$, $P3(x3, y3, z3)$, and $P(x, y, z)$ are positions of globular joints of 5th, 6th, 1st, and 4th leg, respectively. First, from the points, P_1 and P_3, h can be calculated as followings.

$$\begin{aligned} h &= 2h_0 = \overline{PP_3} \\ &= \sqrt{(x_1-x_3)^2+(y_1-y_3)^2+(z_1-z_3)^2-3l_p^2}. \end{aligned} \tag{19}$$

TABLE I

Given pose to find ΔL_x, ΔL_y, and ΔL_z(θ_{b2} and θ_p : $0°$ for 1st and 4th leg, $120°$ for 2st and 5th leg, $240°$ for 3st and 6th leg.)

l_0	50.0	x	0.0
l_b	10.0	y	0.0
l_1	7.0	z	25.0
h_0	7.0	θ_x	0.0°
θ_{b2}	0°,120°,240°	θ_y	0.0°
θ_p	0°,120°,240°	θ_g	0.0°
l_x	$l_b/cos\theta_t$	θ_t	30.0°
l_t	$l_b/sin\theta_t$		

TABLE II

Given pose to find ΔL_x, ΔL_y, and ΔL_z

Variables	Lowest limit	Upper limit	Step
l_2	0.0	20.0	1.0
l_3	0.0	20.0	1.0
l_p	0.0	20.0	1.0
θ_z	0.0	120.0°	15°

The point P can be calculated as

$$\begin{bmatrix} 2(x_2-x_1) & 2(y_2-y_1) & 2(z_2-z_1) \\ 2(x_3-x_2) & 2(y_3-y_2) & 2(z_3-z_2) \\ 2(x_1-x_3) & 2(y_1-y_3) & 2(z_1-z_3) \end{bmatrix} \begin{bmatrix} x \\ y \\ z \end{bmatrix} = \begin{bmatrix} x_2^2+y_2^2+z_2^2-(x_1^2+y_1^2+z_1^2) \\ 3r^2-h^2+(x_3^2+y_3^2+z_3^2)-(x_2^2+y_2^2+z_2^2) \\ h^2-3r^2+(x_1^2+y_1^2+z_1^2)-(x_3^2+y_3^2+z_3^2) \end{bmatrix}. \tag{20}$$

Since P, $P1$, $P2$ are points on a plane, the center of the points and the orientation of the plane can be derived. Finally, the pose of the top plate can be found.

III. Workspace and Optimization

After the kinematic solution, we need to consider workspace. In fact, though a number of parallel type haptic devices have been designed with their own optimization technique, parallel type has so many design factors and complex characteristics that there is no general cost function, fundamentally for the optimization of workspace.

A. Link Ratio and Initial Orientation Optimization

Optimization of PATHOS-II is to maximize workspace under constraint of link lengths. The most important factor which affects the volume of workspace is link ratio and initial orientation. Therefore, in order to maximize the workspace, cost function which is dependent on l_2, l_3, l_p, and initial orientation about z axis, θ_z, is selected as the following.

$$G(l_2, l_3, l_p, \theta_z) = \frac{\Delta L_x + \Delta L_y + \Delta L_z}{(l_2+l_3+l_p)/3} \tag{21}$$

First, system parameters and initial pose except l_2, l_3, l_p and θ_z are fixed as shown in Table I. The parameters in Table I is explained in Figure 3. x, y, z, θ_x, and θ_y are initial pose. ΔL_x, ΔL_y, and ΔL_z in Eq.(21) denote movable ranges in x, y, and z direction in which inverse kinematics solution exists continuously. The numerator means the workspace and the denominator keeps the cost function from being larger as links become longer. The value of cost function is calculated by increasing l_2, l_3, l_p and θ_z with the steps within ranges in

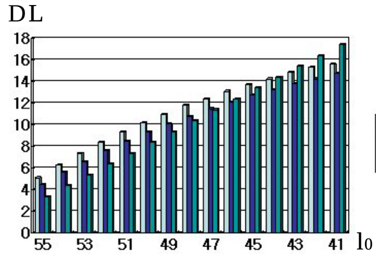

(a)

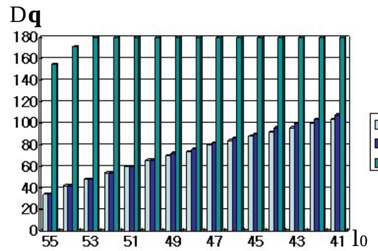

(b)

Fig. 6. (a) : Workspace for fixed initial orientation, (b) : Workspace for fixed initial position

table II. Then, if collision between legs or exceeding the joint angle limit is happened during finding ΔL_x, ΔL_y, and ΔL_z in Eq.(21), the result is excluded. As the result, cost function was maximized when $l_2 = 14.0$, $l_3 = 6.0$, $l_4 = 2.0$ and $\theta_z = 30°$.

B. Workspace

Now, link ratio and initial pose are determined after the optimization of cost function of Eq.(21). However, PATHOS-II is designed to change the length l_0 in Figure 3. Figure 6 shows the workspace when l_0 is changed from 40.0 to 55.0.

ΔL and $\Delta\theta$ in Figure 6 denote the workspace in which inverse kinematics is obtained continuously. For example, ΔL for X in Figure 6(a) is the movable range in x direction when orientation is fixed in initial pose. $\Delta\theta$ for R_x is the rotational range about x axis when position is fixed in initial pose. Figure 6 shows that the workspace is larger as l_0 is smaller. However, for small l_0, space between top plates decreases and collision between human hand and legs is expected. $l_0 = 45.0$ is suitable to avoid collision and maximize workspace.

In fact, the workspace can be increased as the links become longer though link ratio is fixed. So, the workspace is compared to the haptic device size. The dimension of PATHOS-II is a cylinder shape of $20.0cm$ diameter and $45.0cm$ height and the workspace is about a sphere of $14.0cm$ diameter which can cover the human haptic manipulation range[7]. However, this reachable workspace cannot be used before manipulability and isotropy are considered. In the case of PATHOS-II, this reachable workspace can be almost used in the view point of isotropy. It will be explained in the next section.

IV. Isotropy

Another important requirement for a good haptic device is isotropy which makes a haptic device move to any direction an operator wants or guarantees similar stiffness of an haptic device toward every direction.

$$\dot{\boldsymbol{x}} = \boldsymbol{J}\dot{\boldsymbol{q}}, \tag{22}$$

TABLE III
Initial pose of PATHOS-II

x	y	z	θ_x	θ_y	θ_z	l_0	h_0
0.0	0.0	22.5	0.0°	0.0°	30°	45.0	7.0

where

$$\begin{aligned} \dot{\boldsymbol{x}} &= [\dot{x} \;\; \dot{y} \;\; \dot{z} \;\; \omega_x \;\; \omega_y \;\; \omega_z]^T, \\ \boldsymbol{J} &= [\boldsymbol{J}_p^T \; \boldsymbol{J}_o^T]^T, \\ \dot{\boldsymbol{q}} &= [\dot{q}_1 \;\; \dot{q}_2 \;\; \dot{q}_3 \;\; \dot{q}_4 \;\; \dot{q}_5 \;\; \dot{q}_6]^T. \end{aligned} \tag{23}$$

$$\begin{aligned} \delta\boldsymbol{q}^T \cdot \boldsymbol{\tau} &= \delta\boldsymbol{x}^T \cdot \boldsymbol{F}, \\ \boldsymbol{\tau} &= \boldsymbol{J}^T\boldsymbol{F}. \end{aligned} \tag{24}$$

Eq.(22) and (24) show velocity and force relations between task and joint space. $\dot{\boldsymbol{x}}$ and $\dot{\boldsymbol{q}}$ mean velocities of task coordinate and active joint. Though PATHOS-II has 7-DOF, since h_0 is constant when an operator grasps an object, it is reasonable to consider 6-DOF spatial task space. The jacobian, $\boldsymbol{J}$, is decomposed to $\boldsymbol{J}_p$ and $\boldsymbol{J}_o$ which are 3×6 matrices related to velocity and angular velocity since position and orientation have different dimensions. After singular value decomposition, condition number which is the ratio of maximum and minimum singular values means isotropy of velocity and angular velocity or force and moment. For example, if condition number is close to 1, system is isotropic at the attitude. If its condition number becomes large or singular, the haptic device is not a structure any more, since force reflection is not available. To be a nice haptic device, it should be isotropic in every attitude in its workspace.

Though PATHOS-II is designed to have symmetric structure for isotropy, the stiffness in Z direction in Figure 3 can be lower than other directions if the direction vector of active joints is aligned to Z direction. So, θ_t needs to be determined to make PATHOS-II have similar stiffness in every direction and θ_t is selected as $30°$.

Condition numbers of PATHOS-II in 6 plane are shown in Figure 7 and 8 which are obtained from J_p and J_o, respectively. (b), (d), and (f) are projection images of (a), (c), and (e) to the plane. For example, to draw (a) and (b) in Figure 7, condition number of J_p is calculated with the initial pose of PATHOS-II in Table III at every point by increasing x and y by 0.1 in reachable workspace.

From Figure 7 and 8, the condition number is less than 5 for the most part of workspace. However, the condition numbers increase sharply near workspace boundaries. In x-y plane, reasonable workspace as a haptic device is a circle shape of diameter $12cm$. In y-z plane, PATHOS-II is isotropic in reachable workspace of which the length of the major and minor axis are $14cm$ and $12cm$, respectively. In x-z plane, the workspace is a circle shape of diameter $12cm$. Therefore, the workspace for haptic display covers almost reachable workspace.

V. Experiment and Stiffness

In order to display impedance of virtual environment accurately, a haptic device should have a capability to generate high impedance as mush as possible. For example, a haptic device should follow the position of virtual environment or create

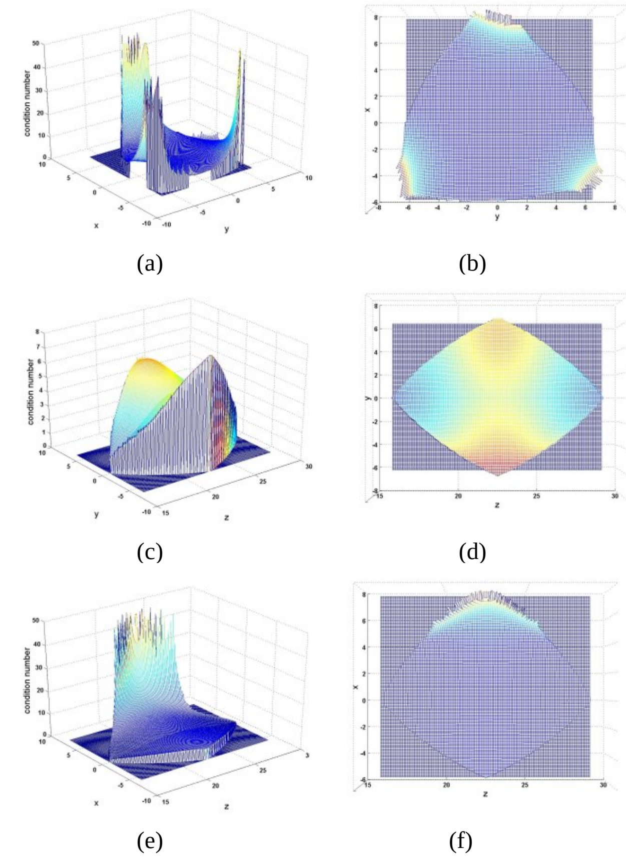

Fig. 7. Condition numbers of J_p (a) : x-y, (b) : projection (a) to x-y plane ,(c) : y-z ,(d) : projection (c) to y-z plane ,(e) : x-z ,(f): projection (e) to x-z plane

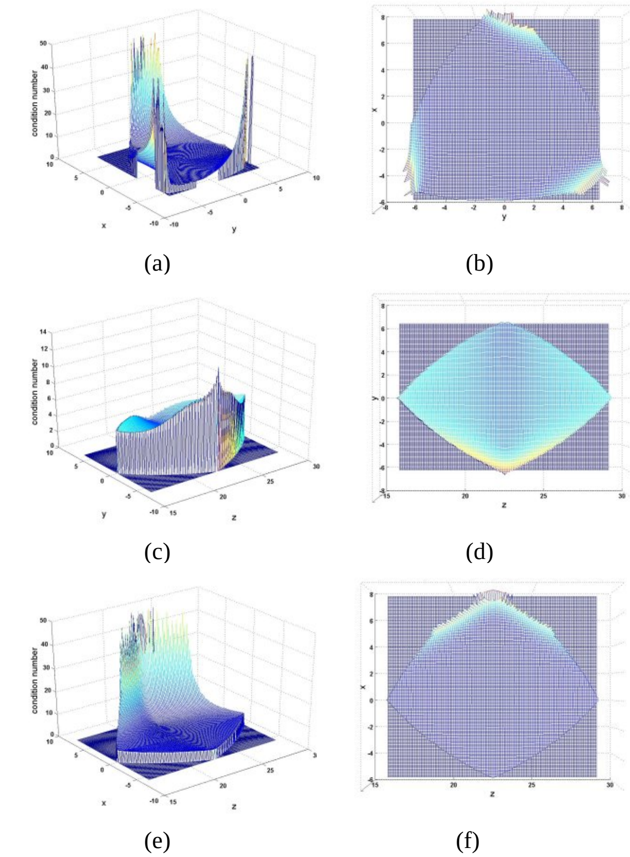

Fig. 8. Condition numbers of J_o (a) : x-y, (b) : projection (a) to x-y plane ,(c) : y-z ,(d) : projection (c) to y-z plane ,(e) : x-z ,(f): projection (e) to x-z plane

reflection force under any human force. Such abilities depend on stiffness of a haptic device. PATHOS-II has high stiffness and accuracy since it has parallel structure. Following experiment shows the stiffness characteristics of PATHOS-II.

A. Experimental System

For the experiment, Pentium-IV PC-1.0GHz and RTX 4.0 based on WIN-NT 4.0 are used. The control frequency is 1.0kHz. 90Watt Maxon motors with $26 : 1$ gear ratio are used for the first active joint of each leg. D/A and encoder counter boards of Sensoray S626 are used. ATI 6-DOF force-torque sensor is used.

When an operator grasps an object tightly, h_0 is fixed and PATHOS-II becomes 6-DOF. In order to know the stiffness limitation of this status, the distance between top plates, h_0 in Figure 3 is fixed as 7.0. The force sensor is equipped on top plate as shown in Figure 10.

In this experiment, PATHOS-II will be used as a master device in two-port admittance haptic interface as shown in Figure 9. F_h and v_h denote force and velocity of human. F_e is the force transmitted to a virtual object and v_e is the velocity of an object in virtual environment. Zero-order hold and digitizer connect the real and virtual world. K denotes controller and F_d is the force generated by K to control the velocity of a haptic device. Virtual coupling is a filter to guarantee passivity of haptic interface[9].

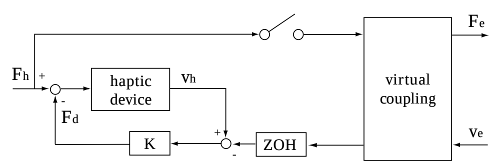

Fig. 9. Structure of Admittance haptic display

B. Experiment

The experiment is to verify the stiffness of PATHOS-II in grasping status of an virtual object. In order to know the characteristics of PATHOS-II and minimize the effects of virtual coupling and controller, virtual coupling is removed and stiffness test is executed in virtual environment with static impedance. v_e is forced to zero so that the maximum impedance or stiffness is established. Then the value of impedance, F_e/v_e, or the stiffness, F_e/p_e, where $p_e = \int v_e dt$, of virtual environment becomes infinity. If a haptic device displays the impedance perfectly, its position, $p_h = \int v_h dt$, maintains zero when human force, F_h, is applied to a haptic device. However, since any haptic device can not display infinite impedance or stiffness, it is important to design a haptic device so that the variation of p_h is smaller in this experiment.

An operator grasps the handle at the initial pose in Table III and push it toward X, Y, and Z direction with respect to the reference coordinate in Figure 3. The desired position

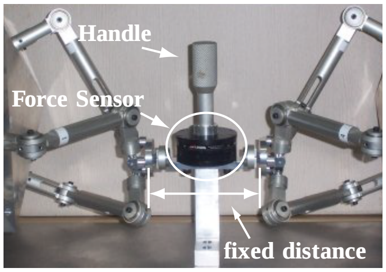

Fig. 10. PATHOS-II for Stiffness Experiment

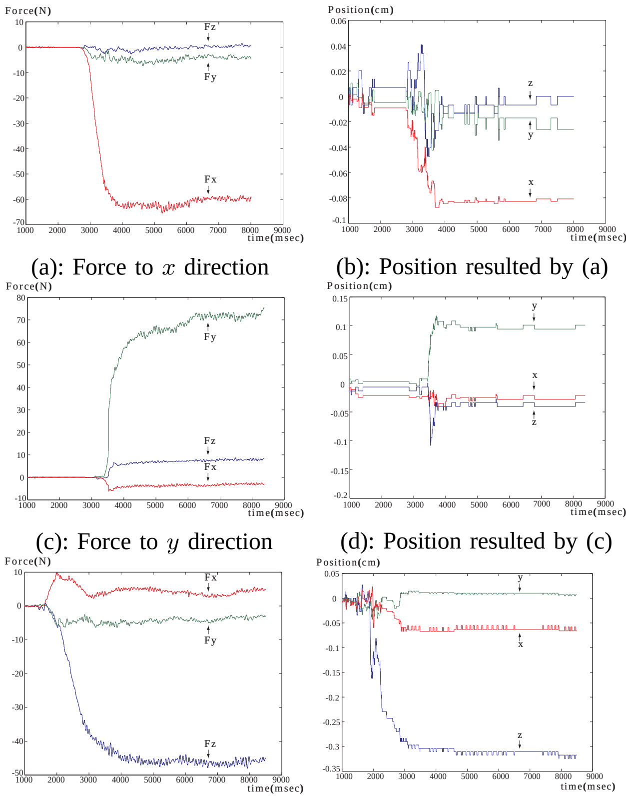

(a): Force to x direction (b): Position resulted by (a)

(c): Force to y direction (d): Position resulted by (c)

(e): Force to z direction (f): Position resulted by (e)

Fig. 11. Experimental Results of Stiffness Test

and velocity of PATHOS-II is zero since the stiffness of virtual environment is infinite.

Figure 11 shows the result of the experiment. (a), (c), and (e) are human force. (b), (d), and (f) are variation of the end effector under the force in (a), (c), and (e). Table IV shows the stiffness of PATHOS-II. It is strong enough to display the high impedance of virtual environment and PATHOS-II maintains the desired position under high disturbance.

VI. Conclusion

The proposed haptic device PATHOS-II enables 6-DOF manipulation and 1-DOF grasping. The inverse kinematics was simple and the forward kinematics was solved using 9 sensors. The workspace was optimized to maximize it under the constraint of link length. The link ratio and initial orientation was used to do this. Another strong point of PATHOS-II is the enhanced isotropic manipulability in most reachable workspace due to its symmetric structure. PATHOS-II is designed to have parallel structure in order to guarantee high stiffness and accuracy. Experimental results verified that it has the capacity to display impedance of virtual environment accurately with its high stiffness. It is expected that PATHOS-II can be used effectively as a haptic device for manipulating an object in many applications, including micro-tele operation.

TABLE IV
Stiffness of PATHOS-II

Direction	x	y	z
Stiffness(N/m)	72000	70000	17000

Acknowledgements

This work was supported by grant No. 2000-2-30200-008-3 from the Basic Research Program of the Korea Science & Engineering Foundation and No. 02-PJ3-PG6-EV04-0003 from of the Korea Health 21 R&D Project, Ministry of Health & Welfare, Republic of Korea.

VII. References

[1] M. Bouzit, G. Burdea, G. Popescu, and R. Boian, “The Rutgers MasterII-New Design Force-Feedback Glove,” IEEE/ASME Trans. on Mechatronics, vol. 7, pp. 256-263, June, 2002.

[2] Sooyong Lee, Jangwook Lee, Woojin Chung, Munsang Kim, Chongwon Lee, and Mignon Park,“ A new exoskeleton-type masterarm with force reflection : Controller and integration,” *Proc. of 1999 IEEE/RSJ International Conference on Intelligent Robots and Systems*, pp. 1438–1443, Victoria, Canada, October 1999.

[3] T. Massie, K. Salisbury, “PHANToM Haptic Interface: A Device for Probing Virtual Objects,” *ASME Journal of Dynamic System and Control*, New York, pp.295-299, 1994.

[4] J.H. Lee, K.S. Eom, B.J. Yi, and I.H. Suh, “Design of A New 6-DOF Parallel Haptic Device,” *Proc. of the IEEE International Conference on Robotics and Automation*, pp.886-891, Seoul, Korea, May 21-26, 2001.

[5] P. Berkelman and R. Hollis, “Lorentz magnetic levitation for haptic interaction: Device design, performance, and integration with physical simulations,” *The International Journal of Robotics Research*, vol. 19, pp. 644-667, July, 2000.

[6] F. Freudenstein, E.R. Maki, “ The creation of mechanisms according to kinematic structure and function,” Environment and Planning B, 1979, pp. 375-391, Vol 6.

[7] Keehoon Kim, Y. Youm, and W.K. Chung, “Human Kinematic Factor for Haptic Manipulation : The Wrist to Thumb,” *10th International Symposium on Haptic Interfaces for Virtual Environment and Teleoperator System*, March 24-25, 2002, pp. 319-326

[8] Keehoon Kim, “Design and Control of 6-DOF Parallel Manipulator for Haptic Display,” Thesis of Master Degree, Pohang University of Science and Technology 2001.

[9] R. J. Adams and B. Hannaford,“Stable Haptic Interaction with Virtual Environments,” *IEEE Trans. on Robotics and Automation*, Vol.15, No.3, pp.465-474, June, 1999.